

PARTICLE SIZE EFFECTS ON THE PHOTOCATALYTIC ACTIVITY OF BiFeO₃ PARTICLES

B. P. REDDY, V. RAJENDAR, M. C. SHEKAR, S. H. PARK*

Department of Electronic Engineering, Yeungnam University, 280 Daehak-ro, Gyeongsan-si, Gyeongsangbuk-do, South Korea

To investigate particle size effect on the photocatalytic activity of BiFeO₃ (BFO), phase pure BFO particles with different average grain sizes were prepared by using facile sol gel route. The X-ray diffraction, Scanning electron microscopy, photoelectron spectroscopy and UV-vis-NIR spectroscopy measurements were used to analyze the as prepared BFO particles. The photocatalytic activities of as-prepared BFO particles were analyzed by the photodegradation of model Rhodamine B(RhB) pollutant under visible light irradiation. The analysis show that crystal defects and surface area plays major role in photocatalytic degradation. In present case BFO particles with average grain size 190 nm has shown better catalytic activity towards degradation of RhB pollutant.

(Received October 13, 2017; Accepted January 14, 2018)

Keywords: Sol-gel, BiFeO₃ particles, Photocatalysis

1. Introduction

Ever since the discovery of water splitting under irradiation of sunlight by Fujishima in 1972, the semiconductor photocatalysis have been received great attention due to its widespread application in waste water treatment and hydrogen production[1]. In photocatalysis, the photocatalysts absorb solar energy and directly converts it into chemical energy showing an ecofriendly way for harvesting renewable energy [2-3]. Several wide band-gap semiconducting photocatalyst materials such as TiO₂ (3.3 eV), ZnO (3.4 eV), ZnS (3.6 eV), SrTiO₃ (2.97 eV), and α -Fe₂O₃ (2.67 eV) are studied extensively for photocatalysis [4-9]. Because of their wide bandgap these photocatalysts can only access to the photons from UV region of solar spectrum, which accounts a maximum of 5% of the total solar energy irradiation, which greatly limits its practical applications[10]. Hence, the research has been focused on the development of visible light driven photocatalyst materials.

During photocatalysis, the e⁻ - h⁺ pairs that are generated upon excitation of photocatalyst are migrated to the interface to form oxidizing species. These migrated electrons are responsible to generate superoxide anion radicals while holes are responsible for the generation of OH[•] radicals that can degrade various organic compounds. If the initial spatial resolution of the charge carriers within a semiconductor is very short then the electron and hole recombination occurs quickly and degrades the performance of the photocatalyst. Thus in order to achieve high yield, a photocatalyst must be highly capable of electron-hole pair separation and good optical absorption properties[11].

As a multi-functional material BiFeO₃ (BFO) which belongs to multiferroic group of materials, in which coexist ferro electricity and ferro magnetism above room temperature, has drawn special attention for its wide range of potential applications in the fields of sensors, spintronics, data storage technology, ferroelectric field effect transistors (FEFET) etc[12-14]. Because of its narrow band gap (2.2 eV) which falls in visible region, low cost and excellent chemical stability over a wide range of pH the research now has been focused on the visible light driven photocatalytic activity of BFO, such as solar water splitting and waste water treatment[15-

* Corresponding author: sihyun_park@ynu.ac.kr

16]. It has been reported that, the strong spontaneous polarization ($6.1 \mu\text{C cm}^{-2}$) present in ferroelectric domains along $\langle 111 \rangle$ direction of BFO leads to band bending which drives the photo generated electrons and holes to opposite directions [17-18]. As a result the charge carriers are spatially resolved and are less prone to recombine and this may enhance the photocatalytic ability of BFO. The narrow band gap and strong spontaneous polarization allows carrier excitation in BFO under visible light irradiation, and hence enables us to develop BFO-based visible-light driven photocatalysts.

Among various synthesis techniques, sol gel technique is widely used to synthesize BFO material due its low cost equipment, ease of preparation and one can achieve uniform composition at relatively low temperatures [3, 19-21]. Despite the reports are available on the sol gel synthesized BFO nano particles there are very few reports are available on the particle size effects on photocatalytic properties of BFO particles [22-23]. In present study, different sizes of BFO particles were prepared and the role of particle size on the photocatalytic activity of BFO particles has been investigated.

2. Experimental

2.1. Preparation of BFO particles

BFO particles were synthesized via simple sol gel technique. All the chemicals are of analytical grade purchased from Dukson chemicals and used without any further modification. In present synthesis, 0.02M of Citric acid/EDTA (Ethylenediaminetetraacetic acid) and equimolar amounts (0.01M) of Bismuth (III) nitrate pentahydrate ($\text{Bi}(\text{NO}_3)_3 \cdot 5\text{H}_2\text{O}$) (purity $\geq 99.0\%$) and Iron(III) nitrate nonahydrate $\text{Fe}(\text{NO}_3)_3 \cdot 9\text{H}_2\text{O}$ (purity 99.0%) were dissolved in to 200mL of water to prepare precursor solution. After vigorous stirring of the solution at 70°C for two hours, ethylene glycol was added to the solution and kept it for ten minutes. The solution was then dried by keeping the solution at 100°C for 12 hrs, which was subsequently grinded into powders. The as-prepared powders were then subjected to annealing in the range from 400°C to 700°C to form BFO particles. The prepared BFO particles were then treated with diluted HNO_3 to remove any impurity phases present in the BFO powders. The prepared BFO particles were coded as C-BFO- T_a , E-BFO- T_a (where T_a is annealing temperature) for the powders prepared using Citric acid, EDTA respectively.

2.2. Characterization of BFO particles

The crystal structure and phase of the prepared samples were examined using PAN analytical X'Pert PRO X-ray diffractometer (XRD) using $\text{Cu } k_\alpha$ radiation. The surface morphology features and composition of the prepared samples films were probed by Hitachi S-4200 field emission scanning electron microscope equipped with energy dispersive X-ray spectrometer (Oxford Instruments, INCA 250). The chemical states of the elements presented in the samples were investigated by using Thermo Scientific X-ray photoelectron spectrometer (Model: K-ALPHA surface analysis) with $\text{Al } k_\alpha$ radiation. The optical properties were determined by using Varian Cary 5000UV-Vis-NIR double beam spectrophotometer.

2.3. Photocatalytic activity of BFO particles

The photocatalytic activities of as-prepared BFO particles for photo degradation of Rhodamine B (RhB) were evaluated under visible light ($\lambda \geq 420 \text{ nm}$) using a 50 W warm white light LED lamp as a light source. In each experiment 10mg of photocatalyst was suspended in 100 ml of RhB solution (5 ppm) and stirred in dark for one hour to attain the adsorption-desorption equilibrium. Then the suspension was exposed to visible irradiation under constant stirring and 4 mL of suspension was collected at regular intervals of time from the reactor. The suspension was filtered using PTFE Whatman filters for removing any photocatalyst present in the suspension and the resulting suspension were then used to study photo degradation process of RhB by measuring the absorbance at 554 nm.

3. Results and discussion

3.1. Structural studies

Fig 1 shows the XRD profiles of as prepared BFO particles at different annealing temperatures. All samples exhibits the major diffraction peaks that are corresponding to rhombohedral BFO (R3C space group) (JCPDS card no: 74-2016). The presence of minor peaks in the samples C-BFO-400, C-BFO-500 indicate the existence of secondary phases like $\text{Bi}_2\text{Fe}_4\text{O}_9$. The intense and sharp diffraction peaks that are resulted from XRD indicates the samples were highly crystalline in nature. The observations revealed that the intensity of diffraction peaks which is directly related to crystallite size of the samples tend to increase with increase in temperature and this trend was more favorable in case of BFO samples prepared using EDTA than the samples prepared using citric acid. Using X'pert Highscore plus, the Rietveld refinements of XRD patterns were performed and results were given in table.1. The results reveal that there was no much changes in c/a ratio observed and is nearly constant irrespective annealing temperature used in the preparation of BFO particles. Therefore it was believed that the static polarization which proportional to square root of the distortion (c/a ratio) remains unchanged with in studied particle size range[22].By inspecting fig.2 we notice that with downscaling of BFO particles peak broadening of (104) and (110) has increased and peaks shifted slightly towards higher angle side. This may be due to local compressive strain due to down scaling of BFO particles. The estimated values of local inhomogeneous strain (table.1) also confirms that the downscaling of crystallite size results in enhancement of inhomogeneous strain pertaining to the defects. A similar shift and broadening was observed in all reflections with downscaling of BFO particles.

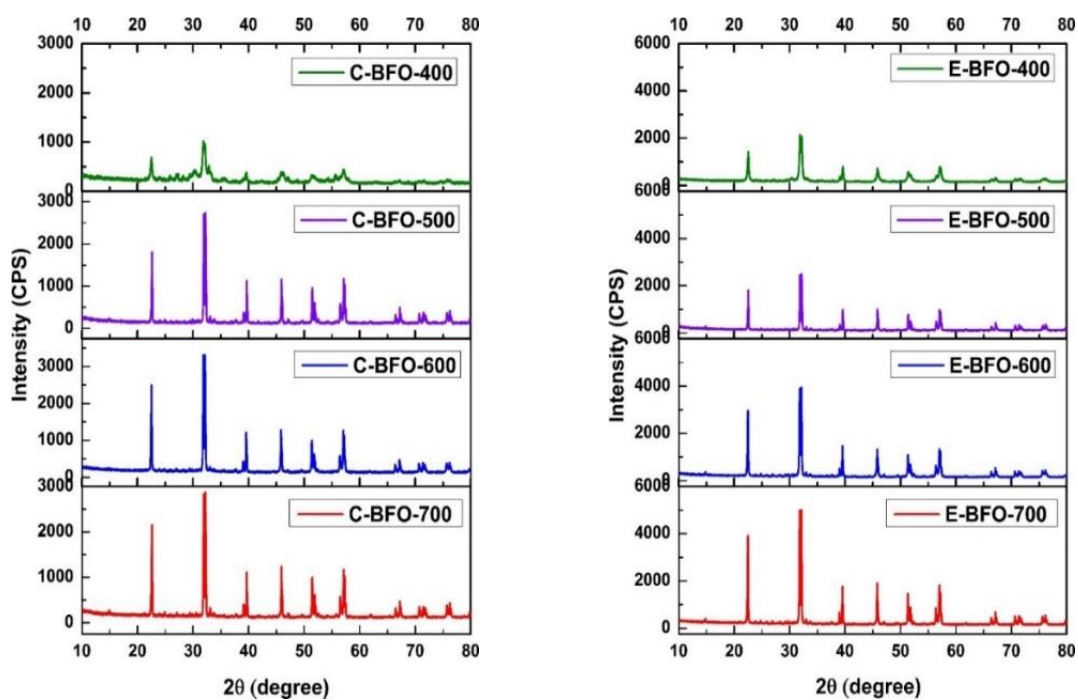


Fig.1. XRD profiles of prepared BFO particles

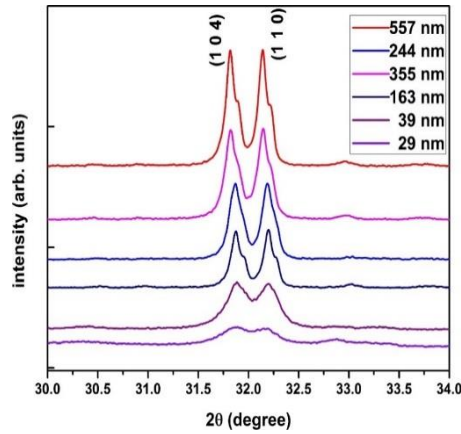


Fig.2. Peak broadening of Bragg peaks with respect to crystallite size

Table.1 Physical parameters of the BFO particles calculated from XRD and SEM measurements

Sample name	Lattice constants		c/a	Distortion (c-a)/c	Crystallite size (nm)	Grain Size (nm)	Strain(ϵ) ($\times 10^{-4} \text{m}^{-2}$)	Bi/Fe ratio (EDAX)
	a	c						
E-BFO-700	5.5798	13.8732	2.4863	0.5978	557	615	3.83	1.033
E-BFO-600	5.5817	13.8797	2.4867	0.5978	355	423	4.00	1.024
C-BFO-700	5.5808	13.8776	2.4866	0.5978	306	378	4.032	1.004
E-BFO-500	5.5787	13.8701	2.4862	0.5977	244	295	4.26	1.086
C-BFO-600	5.5797	13.8740	2.4865	0.5978	198	225	4.84	1.054
C-BFO-500	5.5783	13.8694	2.4863	0.5977	163	190	5.23	1.073
E-BFO-400	5.5805	13.8712	2.4856	0.5976	39	67	13.87	1.141
C-BFO-400	5.5746	13.8621	2.4866	0.5978	29	55	15.24	1.162

3.2. Morphology and composition

Fig. 3 shows the morphological features of prepared BFO particles with respect to annealing temperature. The average grain size of the BFO particles estimated from SEM measurements are tabulated in table 1. The results reveal that the grain size tends to increase with increase in annealing temperature and this phenomena is more prominent in BFO particles derived from EDTA. A closer look on the particle morphology reveals that irrespective of annealing temperature all the particles exhibited similar structure and hence the effects of the morphological changes on the optical properties can be ruled out. For all the BFO particles the ratio of at. % of Bi and Fe (table.1) probed using EDAX are nearly equal to 1 except at lower synthesis temperatures resulted from the presence of impurity phases.

The chemical states of the Bi, Fe and O elements in BFO particles were determined by the XPS analysis. The XPS spectra of the elements presented in fig. 4. The characteristic spectra of Bi 4f reveals two peaks centered at 163.7 and 158.4 which corresponds to Bi 4f_{5/2} and Bi 4f_{7/2} respectively indicating Bi existed in Bi³⁺ state in prepared BFO particles. The presence of peaks at 710 eV and 723.6 eV that are present in Fe 2p spectrum can be attributed to spin orbit interaction. The occurrence of satellite peak at 718.2 eV confirms Fe³⁺ state. The O1s spectra reveals there are three kinds of oxygen species with peak positions signaling at 529.1eV, 530.8 eV and 532.1eV corresponds to lattice oxygen present in BFO layered structure, dangling bond and surface adsorbed oxygen species respectively[24]. Moreover, the quantitative analysis of Bi³⁺ and Fe³⁺ XPS spectra reveals that the atomic ratio of Bi³⁺/Fe³⁺ of prepared BFO particles agree well with crystalline BiFeO₃.

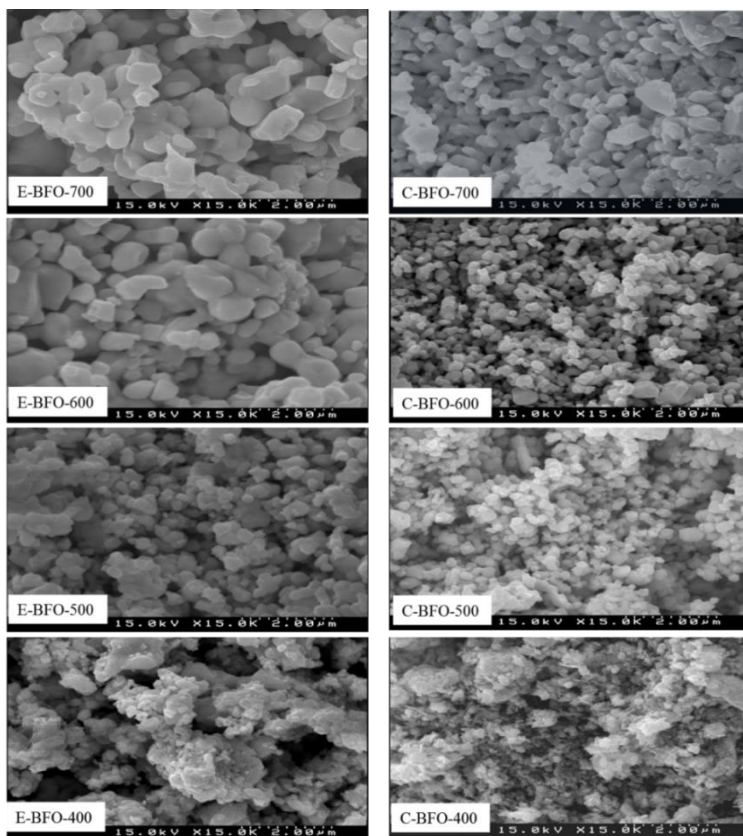


Fig.3. SEM profiles of prepared BFO particles

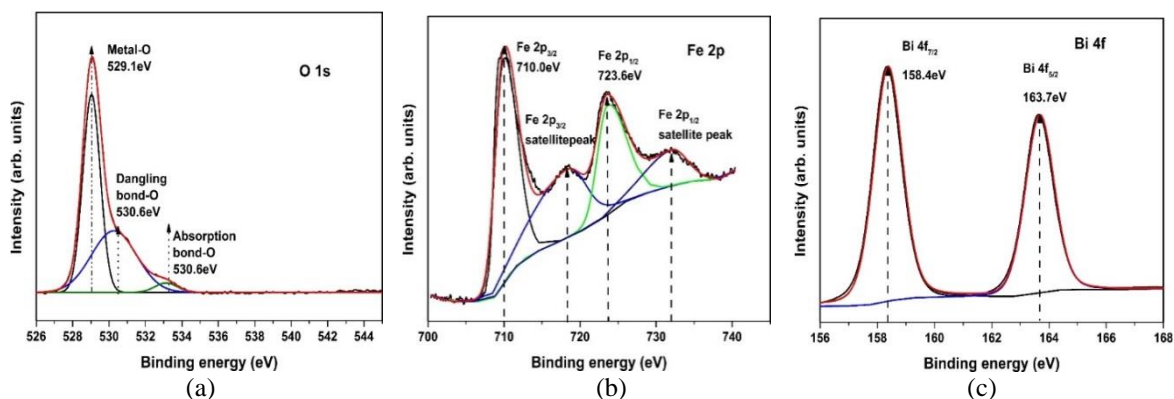


Fig.4. XPS narrow scan spectra of (a) Fe 2p (b) O 1s (c) Bi 4f states of BFO particles with grain size 190 nm.

3.3. Optical properties

To examine the optical properties of BFO, diffuse reflectance spectra of all the BFO particles are studied and are presented in Fig. 5(a). The optical band gap of BFO particles were determined from the plot of $(F(R)h\nu)^{1/2}$ Vs $h\nu$ (fig.5(b)) where $F(R)$ is Kubelka–Munk (K–M) function and R is the reflectance. The observations reveals that the global shape of reflectance spectra of all BFO particles looks similar irrespective of particle size. It has been observed that the optical band gap of the all BFO samples (Fig.5b) lies in the visible range and were in the range of 2.3 eV to 2.45 eV which is quite less than in bulk crystals. However the optical bandgap of the BFO particles increases with decreasing particle size. Below 2.1 eV, there are two other bands at

1.9 eV and below 1.5eV are observed in the fig 5(b) which can be attributed to magnetically sensitive transitions originating from ${}^6A_{1g}$ to ${}^4T_{1g}$ and ${}^4T_{2g}$ respectively[22]. With the downscaling of BFO particles the intensity corresponds to these bands found to be decreased. This may be due to the defects that are present in the particles which leads to distortion of local symmetry. Thus these transitions are mainly affected by the downscaling of BFO particles.

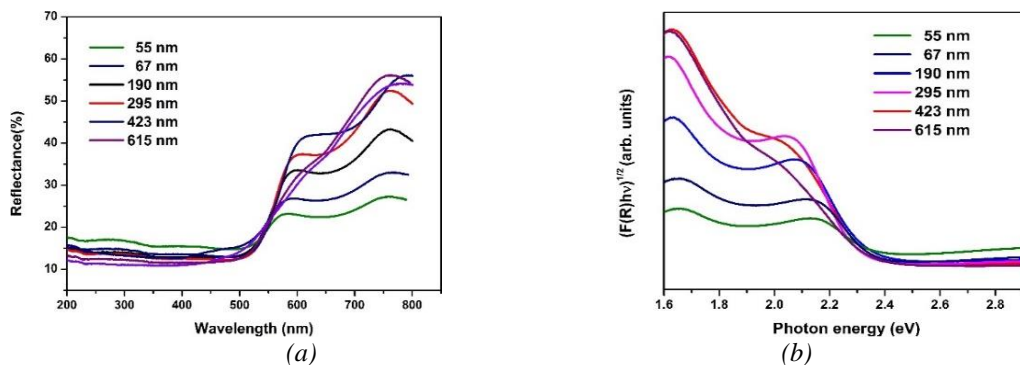


Fig.5. (a) Dependence of reflectance with grain size of BFO particles and (b) corresponding plots of $(F(R)h\nu)^{1/2}$ Vs $h\nu$

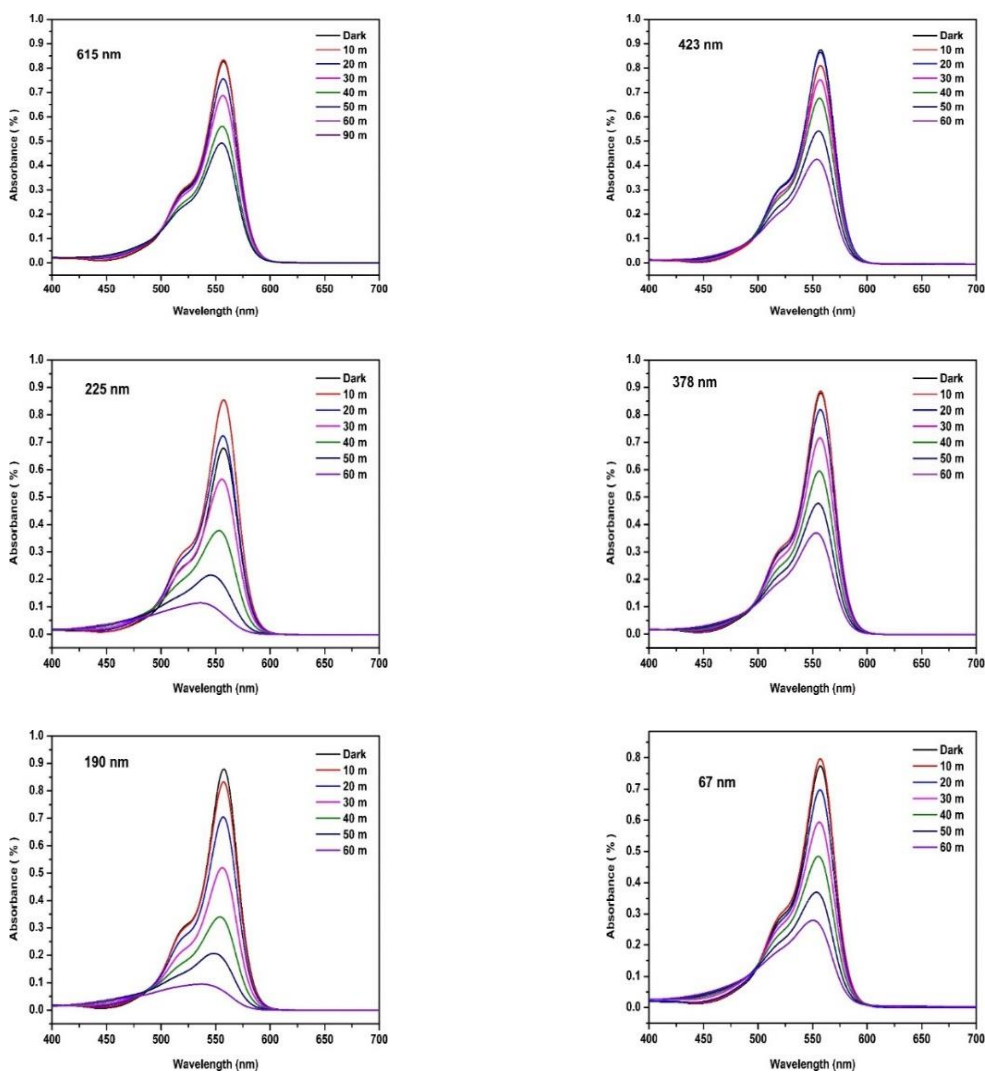


Fig.6. Absorption spectra of RhB with respect to time in presence of BFO photocatalyst of different grain sizes under visible light irradiation

3.4. Photocatalytic activity

The photocatalytic degradation experiments were carried out using model RhB as pollutant in presence of BFO photo catalyst while maintaining pH value at 2.9 and the results were presented in Fig.6. The photo degradation experiments clearly reveals that under visible light irradiation the absorbance peak intensity that corresponds to RhB decreases as the time progress indicating that RhB has been degraded by BFO. One can also find that the rate of decrease of RhB absorbance peak intensity was maximum for the BFO with average particle size 193nm. A blue shift in the peak position that correspond to RhB has been blue shifted as the time progress indicating the formation of intermediate species due to the conversion of triethylrhodamine to diethylrhodamine. It has been observed that the peak position In order to find out photo degradation efficiency of RhB by BFO particles, C_t/C_0 values were calculated (C_0 and C_t are maximum intensity of RhB absorbance peak considered at times $t=0$ and $t=t$ respectively) and plotted against time (Fig.7(a)). It has been observed from fig.7 that the rate of degradation has been accelerated nearly 80% upon addition of photocatalyst. And also as the size of BFO particles decreases from 615 nm to 190 nm the efficiency found to be increased however a further downscaling of BFO particles results in less efficiency. To understand photo degradation kinetics the rate constants (k) were determined by measuring the slopes from curves $\ln(C_t/C_0)$ plotted against time (Fig.7(b)). Fig 8 shows a clear deviation of the plot from straight line for all samples which indicates three different stages of degradation. An initial linear decay and then a transition stage which followed by linear decay. The rate constants that are corresponds to the first stage and last stage are given in table 2. The different rate constants that are observed in the fig.8 may corresponds to degradation of triethylrhodamine and diethylrhodamine[25]. The results reveal that as the particle size decreases from 615 nm to 190 nm the rate constant values increases monotonically and a further downscaling to 29 nm the rate constant again decreases.

In general, the decrease in particle size leads to the quadratic growth of active surface area which in turn enhances the number of foreign species that react the surface and resulting in increased photocatalytic activity. This is true in our case as the particle size decreases from 615 nm to 190 nm the degradation efficiency increased from 15% to 30%. And also as the particle morphology looks similar in nature hence the effects of variation in static polarization and to the better absorption of light from specific planes has a minimal contribution to the specific increment in degradation efficiency. Hence the increase in specific reaction area with downscaling of BFO particles is the prime cause for the observed improvement in photocatalytic activity. However the scenario has been changed with further decrease in particle size below 190 nm. The number of defects and the corresponding local inhomogeneous strains revealed by broadening of Bragg peaks are increased nearly by tenfold with downscaling from 190 nm to 30 nm. If these defects present on the surface, they may act as a recombination centers for charge carriers and resulted in less efficiency of the BFO particles. If these defects present inside the particles, they indeed act as a trapping centers for e^- and h^+ and act as barriers which prevent migration of charge carriers towards surface there by decreasing the efficiency.

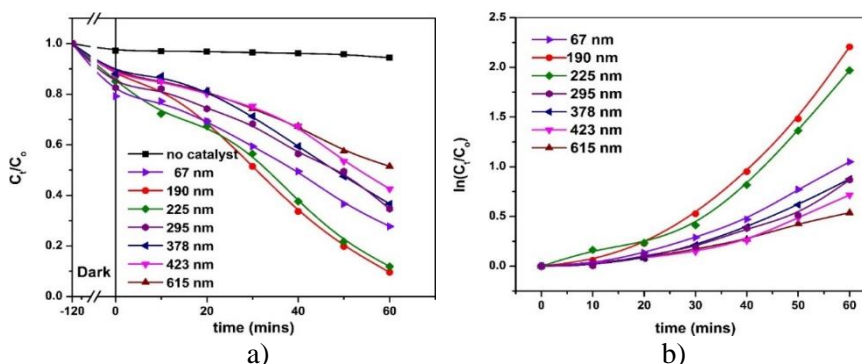


Fig.7. (a) Photo degradation and (b) Photo degradation kinetics of RhB in presence of BFO photocatalyst

Table.2 Dependence of Band gap, degradation efficiency and Rate constants of BFO particles on the particle size

Grain Size (nm)	Optical band gap (eV)	$(C_0 - C_t)/C_0$ (%) After 40 mins	Rate constants	
			k1 ($\times 10^{-3} \text{ min}^{-1}$)	k2 ($\times 10^{-2} \text{ min}^{-1}$)
615	2.38	42	5	1.16
423	2.40	46	5.6	1.93
378	2.41	47	6.7	2.17
295	2.41	52	7.07	2.2
225	2.44	78	13.05	5.22
190	2.47	80	18	5.6
67	2.48	63	9.7	2.59

4. Conclusions

In summary, phase pure BFO particles of different average grain sizes were prepared by using sol gel technique. The grain size was tailored by adding either citric acid or EDTA and annealing at different temperatures. The XRD studies reveal that there was no much changes in c/a ratio and in static polarization values and remains unchanged with in studied particle size range. There are no substantial morphological changes observed with decreasing the grain size of BFO particles. The optical band of BFO particles lies in the visible range and the bandgap increases with decreasing particle size.

The photocatalytic degradation experiments reveal that as the particle size decreases from 615 nm to 190 nm the rate constant values increases monotonically and a further downscaling to 29 nm the rate constant again decreases. The results reveal that the photocatalytic activity of the BFO particles mainly depends on the crystal defects, local homogeneous strain and active surface area which in turn depends on the grain size. Thus by tuning the grain size of BFO particles one can enhance the photocatalytic efficiency of BFO particles.

Acknowledgement

This work was supported by Human Resources Program in the Transportation Specialized Lighting Core Technology Development (No. N0001364) granted financial resource from the Ministry of Trade, Industry & Energy, Republic of Korea.

References

- [1] A. Fujishima, K. Honda, *Nature* **238** (5358), 37 (1972)
- [2] S. Irfan, L. Li, A. S. Saleemi, C.-W. Nan, *Journal of Materials Chemistry A* **5**(22), 11143 (2017)
- [3] T. Gao, Z. Chen, Y. Zhu, F. Niu, Q. Huang, L. Qin, X. Sun, Y. Huang, *Materials Research Bulletin* **59**, 6 (2014)
- [4] J. J. M. Vequizo, H. Matsunaga, T. Ishiku, S. Kamimura, T. Ohno, A. Yamakata, *ACS Catalysis* **7**(4), 2644 (2017)
- [5] C. Jaramillo-Páez, J. A. Navío, M. C. Hidalgo, M. Macías, *Catalysis Today* **284**(Supplement C), 121 (2017)

- [6] L. Yin ,D. Zhang ,D. Wang ,X. Kong ,J. Huang ,F. Wang , Y. Wu, *Materials Science and Engineering: B* **208**, 15 (2016)
- [7] Z. He ,X.-Y. Sun , X. Gu, *Journal of Materials Science: Materials in Electronics* **28**(18), 13950 (2017)
- [8] M. M. Ba-Abbad ,M. S. Takriff ,A. Benamor , A. W. Mohammad, *Journal of Sol-Gel Science and Technology* **81**(3), 880 (2017)
- [9] C. Jiafeng ,H. Xianshan ,L. Yi ,W. Jianguang , J. Yuexia, *Materials Research Express* **3**(11), 115903 (2016)
- [10] A. Chithambararaj ,N. S. Sanjini ,A. C. Bose , S. Velmathi, *Catalysis Science & Technology* **3**(5), 1405 (2013)
- [11] Q. Chen ,H. Shi ,W. Shi ,Y. Xu , D. Wu, *Catalysis Science & Technology* **2**(6), 1213 (2012)
- [12] M. S. Rahman ,S. Ghose ,L. Hong ,P. Dhungana ,A. Fahami ,J. R. Gatabi, J. S. Rojas-Ramirez ,A. Zakhidov, R. F. Klie, R. K. Pandey, R. Droopad, *Journal of Materials Chemistry C* **4**(43), 10386 (2016)
- [13] T. Tong ,J. Chen ,D. Jin , J. Cheng, *Materials Letters* **197**, 160 (2017)
- [14] D. Chen ,Z. Chen ,Q. He ,J. D. Clarkson ,C. R. Serrao ,A. K. Yadav ,M. E. Nowakowski, Z. Fan, L. You, X. Gao, D. Zeng, L. Chen, A. Y. Borisevich, S. Salahuddin, J.-M. Liu, J. Bokor, *Nano Letters* **17**(1), 486 (2017)
- [15] R. Dhanalakshmi, M. Muneeswaran, P. R. Vanga, M. Ashok, N. V. Giridharan, *Applied Physics A* **122**(1), 13 (2015)
- [16] W. Ji ,K. Yao ,Y.-F. Lim ,Y. C. Liang , A. Suwardi, *Applied Physics Letters* **103**(6), 062901 (2013)
- [17] J. Wang, J. B. Neaton, H. Zheng, V. Nagarajan, S. B. Ogale, B. Liu, D. Viehland, V. Vaithyanathan, D. G. Schlom, U. V. Waghmare, N. A. Spaldin, K. M. Rabe, M. Wuttig, R. Ramesh, *Science* **299**(5613), 1719 (2003)
- [18] H. Yu ,H. Guo ,W. Zhu ,J. Zhuang ,W. Ren , Z.-G. Ye, *Thin Solid Films* **585**, 82 (2015)
- [19] C. Anthonyraj, M. Muneeswaran, S. Gokul Raj, N. V. Giridharan, V. Sivakumar, G. Senguttuvan, *Journal of Materials Science: Materials in Electronics* **26**(1), 49 (2015)
- [20] S. Z. Lu , X. Qi, *Journal of the American Ceramic Society* **97**(7), 2185 (2014)
- [21] A. S. Priya ,I. B. Shameem Banu, M. Shahid Anwar, S. Hussain, *Journal of Sol-Gel Science and Technology* **80**(3), 579 (2016)
- [22] X. Bai, J. Wei, B. Tian, Y. Liu, T. Reiss, N. Guiblin, P. Gemeiner, B. Dkhil, I. C. Infante, *The Journal of Physical Chemistry C* **120**(7), 3595 (2016)
- [23] T. Xian, H. Yang, J. F. Dai, Z. Q. Wei, J. Y. Ma, W. J. Feng, *Materials Letters* **65**(11), 1573 (2011)
- [24] N. Zhang ,D. Chen ,F. Niu ,S. Wang ,L. Qin , Y. Huang, *Scientific Reports* **6**, 26467 (2016)
- [25] M. Rochkind ,S. Pasternak , Y. Paz, *Molecules* **20**(1), 88 (2015)